FORECAST SKILL AND COMPUTATIONAL COST OF THE CORRELATION MODELS IN 3DVAR DATA ASSIMILATION

M. YAREMCHUK*, M. CARRIER, H. NGODOCK,

S. SMITH, and I. SHULMAN

*Naval Research Laboratory,
Stennis Space Center, MS 39529, USA*
E-mail: max.yaremchuk@nrlssc.navy.mil

Many background error correlation (BEC) models in data assimilation are formulated in terms of a positive-definite smoothing operator $\mathbf{B}$ which simulates the action of correlation matrix on a vector in state space. To estimate the efficiency of such approach, numerical experiments with the Gaussian and spline models

$$\mathbf{B} = \exp(\nabla \boldsymbol{\nu} \nabla); \qquad \mathbf{B}_m = \left(\mathbf{I} - \frac{\nabla \boldsymbol{\nu} \nabla}{m} \right)^{-m}$$

have been conducted. Here $\mathbf{I}$ is the identity operator and $\boldsymbol{\nu}$ is the diffusion tensor, whose spatial variability is derived from the forecast field and m is the spline approximation order.

Performance of these BEC representations are compared in the framework of numerical experiments with real 3dVar data assimilation into the Navy Coastal Ocean model (NCOM) in the Western Tropical Pacific. It is shown that both BEC models have similar forecast skills over a two-month time period, whereas the second-order spline model is several times more efficient computationally if the cost function is minimized in the state space.

Keywords: variational data assimilation, covariance modeling

1. Introduction

In recent years, heuristic BEC modelling has become an area of active research in data assimilation (DA). This interest has been fueled by development of the ensemble DA techniques and rapid increase of the data

streams, driven by remotely sensed observations from satellites and introduction of new autonomous observational platforms in oceanography. Traditional BEC models based on the explicit definition of the error covariances by the families of parameterized correlation functions[1,2] tend to loose computational efficiency with the growth of the number of observations and with the necessity to introduce more complex observation operators into the DA algorithms. Because of that, there is a growing tendency to estimate error correlations directly in the model space (MS) or in its subspaces spanned by the appropriately selected basis functions.[3–5].

Of particular interest are the MS correlation models based on positive functions of the diffusion operator $\mathbf{D} = \nabla \nu \nabla$, such as the exponent or the inverse of its binomial approximation[6,7]. Both types of models were extensively used in many applications[8–11] because of their convenience and ease of numerical implementation. Another advantage is their flexibility in approximation of inhomogeneous and anisotropic covariance functions[12,13]. Numerically, these models are implemented by integrating the diffusion equation (DE) using either explicit or implicit scheme.

The computational cost of the DE integration by explicit methods increases substantially when the local decorrelation scale, ρ_c, becomes larger than the model grid step δx. This is because the minimum number of multiplications by $\mathbf{D}$, is proportional to $(\rho_c/\delta x)^2$ – a constraint imposed by numerical stability of the integration. In such situations it may be advantageous to employ implicit integration schemes[11,14], which tend to converge fast enough to deliver considerable computational gain. Additional gain can be obtained if the implicit approximation is implemented within the model space (MS) formulation. In this case, the iterative solution of the system in data space (DS) which embeds an iterative cycle of the implicit scheme, is no longer needed.

This study compares the forecast skill and computational cost of two BEC models: The first model ($\mathcal{C}_\infty$) is described by the propagator of the DE and implemented numerically by its explicit integration; the second BEC model ($\mathcal{C}_m$) is defined by the inverse of a mth-order binomial of $\mathbf{D}$, that approximates $\mathcal{C}_\infty$ and can be interpreted as a result of m-step DE integration with the implicit scheme. Assimilation experiments were performed using both DS and MS formulations of $\mathcal{C}_m$ and a realistic regional ocean model with real data. It is shown that in certain situations it is computationally advantageous to employ the second (spline) model combined with the MS solution to the normal equation.

2. Covariance modelling in MS

2.1. *MS and DS approaches in 3dVar*

In its basic formulation, the 3dVar analysis determines the optimal model state increment $\mathbf{x}$ that minimizes the following cost function,

$$J(\mathbf{x}) = \frac{1}{2} \left[\mathbf{x}^\mathsf{T} \mathbf{B}^{-1} \mathbf{x} + (\mathbf{Hx} - \mathbf{d})^\mathsf{T} \mathbf{R}^{-1} (\mathbf{Hx} - \mathbf{d}) \right] \to \min_{\mathbf{x}}. \qquad (1)$$

Here $\mathbf{B}$ is the BE covariance matrix and $\mathbf{d}$ is the innovation vector

$$\mathbf{d} = \mathbf{y} - \mathbf{Hx}^b$$

where $\mathbf{y}$ denotes observations, $\mathbf{x}_b$ is the background model state, $\mathbf{H}$ is the observation operator (linearized) in the vicinity of $\mathbf{x}_b$, and $\mathbf{R}$ is the covariance matrix of observation errors. To simplify the notation, the variables in both model and data spaces are non-dimensionalized by $\mathbf{x} \leftarrow \mathbf{C}^{-1/2}\mathbf{x}$ and $\mathbf{d} \leftarrow \mathbf{R}^{-1/2}\mathbf{d}$; where $\mathbf{C}$ is the (diagonal) background error variance matrix. In order to keep J invariant, the matrices $\mathbf{B}$, and $\mathbf{H}$ are non-dimensionalized by $\mathbf{B} \leftarrow \mathbf{C}^{-1/2}\mathbf{B}\mathbf{C}^{-1/2}$; $\mathbf{H} \leftarrow \mathbf{R}^{-1/2}\mathbf{H}\mathbf{C}^{1/2}$.

The cost function (1) is minimized by solving the normal equation which sets the gradient of J equal to zero:

$$(\mathbf{B}^{-1} + \mathbf{H}^\mathsf{T}\mathbf{H})\mathbf{x} = \mathbf{H}^\mathsf{T}\mathbf{d}, \qquad (2)$$

so that the solution to the normal equation is:

$$\mathbf{x} = (\mathbf{B}^{-1} + \mathbf{H}^\mathsf{T}\mathbf{H})^{-1}\mathbf{H}^\mathsf{T}\mathbf{d} \qquad (3)$$

Solving equation (2) for the model state increment $\mathbf{x}$ is the basic tool of 3dVar analysis. If $\mathbf{B}^{-1}$ has full rank, the solution (3) is unique and can be rewritten in the dual form[15]:

$$\mathbf{x} = \mathbf{B}\mathbf{H}^\mathsf{T}(\mathbf{H}\mathbf{B}\mathbf{H}^\mathsf{T} + \mathbf{I})^{-1}\mathbf{d} \qquad (4)$$

which is often called the DS solution to the variational problem (1). Note that if $\mathbf{B}^{-1}$ does not have full rank, defining $\mathbf{B}$ as its generalized inverse does not guarantee that solution (4) will coincide with the solution (3) of the original minimization problem. This is because the DS solution (4) is always orthogonal to the null space of $\mathbf{B}$, whereas in general, the minimizer (2) of (1) is not constrained by this condition.

It should also be noted that the majority of the BEC models are based on direct computation of the matrix elements of $\mathbf{B}$ from experimental data,

and therefore, require 3dVar solutions in the forms, involving $\mathbf{B}$. These are the DS solution (4), or the MS solution, preconditioned by $\tilde{\mathbf{B}} = \sqrt{\mathbf{B}}$ [16,17]:

$$\mathbf{x} = \tilde{\mathbf{B}}(\mathbf{I} + \tilde{\mathbf{B}}^\mathsf{T}\mathbf{H}^\mathsf{T}\mathbf{H}\tilde{\mathbf{B}})^{-1}\tilde{\mathbf{B}}\mathbf{H}^\mathsf{T}\mathbf{d} \tag{5}$$

Therefore, the basic MS solution (3) has been used in practice more rarely for two reasons: *a)* it requires solving the linear system in MS, which has many more dimensions than the DS; and *b)* estimation of $\mathbf{B}$ from the data is more straightforward than estimation of $\mathbf{B}^{-1}$.

2.2. *The Gaussian and spline BEC models*

The two types of BEC models considered here are based on the polynomials of $\mathbf{D}$. The major idea is to model the resulting action of the BEC operator $\mathbf{B}$ on a vector $\mathbf{x}$ by integrating the corresponding diffusion equation

$$\frac{\partial \mathbf{x}}{\partial t} = \mathbf{D}\mathbf{x} \equiv \frac{1}{2}\nabla\boldsymbol{\nu}\nabla\mathbf{x} \tag{6}$$

for a certain "time period" T, thus setting $\mathbf{B} = \exp T\mathbf{D}$.

The diffusion tensor $\boldsymbol{\nu}$ is represented by 3×3 positive-definite matrices whose entries depend on the coordinates $\boldsymbol{x}$ in physical space. The eigenvalues $\lambda_i^2, i = 1, ..., 3$ of $\boldsymbol{\nu}T$ are all positive, have the dimension of length squared, and in the homogeneous case ($\boldsymbol{\nu} = const$) they are naturally interpreted as the squares of the decorrelation scales ρ_i in the directions of the respective eigenvectors of $\boldsymbol{\nu}$. In the inhomogeneous case, the decorrelation scales are defined locally in a similar manner, whereas the integration time T plays the role of a global scaling parameter for the distribution of $\rho_i^2(\boldsymbol{x})$. Therefore, setting the value of T is equivalent to specifying the square of the mean decorrelation scale ρ for a given distribution of $\boldsymbol{\nu}(\boldsymbol{x})$. Throughout the remainder of this paper, we keep in mind this equivalence and replace T with ρ^2 where appropriate.

Numerically, the action of the Gaussian BEC operator $\exp(T\mathbf{D})$ is usually represented by integrating (6) with an explicit time-stepping scheme, $\mathbf{x}^{t+\delta t} = \mathbf{x}^t + \delta t\mathbf{D}\mathbf{x}^t$, such that the result of multiplication of a vector $\mathbf{x}^0$ by $\mathbf{B}$ is

$$\mathbf{x}^T \equiv \mathbf{B}\mathbf{x}^0 = \left[\mathbf{I} + \frac{T\mathbf{D}}{n}\right]^n \mathbf{x}^0 \approx \exp[\rho^2\mathbf{D}]\mathbf{x}^0 \tag{7}$$

where $n = T/\delta t$ is the total number of time steps. Expression (7) shows that numerically, the Gaussian BEC model is a high-order polynomial in $\mathbf{D}$. In data assimilation problems the n-step "time integration" (7) is embedded

in the iterative loop that solves linear equations, whose system matrices are under the inversion signs in either (4) or (5). Therefore, reducing n (increasing δt) provides major computational savings. The minimum value for n is limited, however, by the stability condition which constrains eigenvalues of the operator $\mathbf{I} + \rho^2 \mathbf{D}/n$ in (7) not to exceed 1 in magnitude:

$$n \geq \frac{1}{2}\rho^2\lambda \qquad (8)$$

where λ is the absolute value of the largest eigenvalue of $\mathbf{D}$. Numerically, the minimum value of n in 3d is proportional to the square of the largest ratio $\tilde{\rho}$ between decorrellation scale and the local grid step taken over the entire grid. In realistic applications, $\tilde{\rho}$ may easily exceed 10, substantially increasing the cost of computing the action of $\mathbf{B}$ on a vector.

For $\tilde{\rho} > 10$ the computational burden can be reduced by considering a spline BEC model

$$\mathbf{B}_m = \left[\mathbf{I} - \frac{\rho^2\mathbf{D}}{m}\right]^{-m} \simeq \exp[\rho^2\mathbf{D}], \qquad (9)$$

which specifies the inverse BEC as a polynomial in the powers of $-\mathbf{D}$ and converges to the Gaussian model as $m \to \infty$ (Fig. 1).
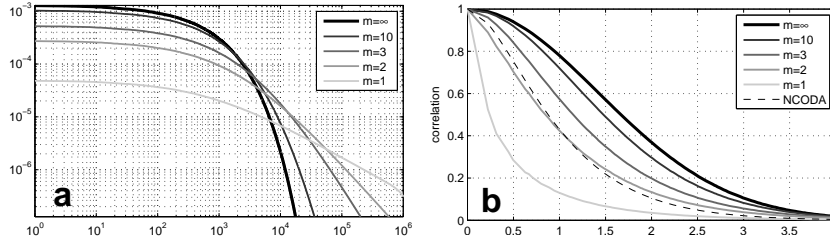
Fig. 1. Normalized spectra of the Gaussian ($m = \infty$) and spline BEC operators with different approximation order m (a) and the corresponding correlation functions (b). Horizontal axis is normalized by the correlation radius. The dashed line shows correlation function used in the experiments with NCODA $\mathcal{C}_d$ model (see Section 3.2).

The BEC operator in (9) can be implemented numerically in two ways, distinguished by the order of the operations of inversion and raising to the mth power. The first method requires m inversions of $\mathbf{I} - \rho^2\mathbf{D}/m$, and this approach can be interpreted as integration of the DE by an implicit scheme[18] with the "time step" $\delta t = \rho^2/m$. The second method involves only one inversion of the matrix whose condition number is c^m, where $c = \text{cond}(\mathbf{I} - \rho^2\mathbf{D}/m)$.

Numerically, each iteration of the first inversion process is approximately equivalent to a one-step integration with the explicit scheme (7) as the corresponding matrices $\mathbf{I}+\rho^2\mathbf{D}/n$ and $\mathbf{I}-\rho^2\mathbf{D}/m$ differ only by the numerical factor before the diffusion operator. The second method of computing the action of $\mathbf{B}_m$ is more expensive than the first one, because the total number of iterations grows exponentially with m, unless an efficient preconditioner is available.

On the other hand, the possibility to directly compute the action of $\mathbf{B}_m^{-1} = (\mathbf{I} - \mathbf{D}/m)^m$ is advantageous in solving the MS 3dVar problem (2), as it requires only one MS iterative cycle to invert $(\mathbf{I} - \mathbf{D}/m)^m + \mathbf{H}^\mathsf{T}\mathbf{H}$. In contrast, the DS solution (4) and the $\tilde{\mathbf{B}}_m$-preconditioned MS solution (5) involve $the\ product$ of two cycles: each iteration of the respective DS/MS system solvers contains an MS iterative cycle required for computing the action of $\mathbf{B}$ (or $\tilde{\mathbf{B}}$) on a vector.

Spectral properties of the low-order spline models differ considerably from the Gaussian one: their spectra exhibit more gentle slopes and weaker damping of the short (near-grid) scales (Fig. 1a) and the correlation functions decay faster than the Gaussian at small distances (Fig. 1b). The difference may affect the forecast skill of the assimilation system and not worth the computational gain when applied to real data. This and other related issues have been examined by means of numerical experimentation.

3. Numerical experiments setup

Experiments were performed with the Relocatable Navy Coastal Ocean Model system (RNCOM) consisting of two primary components: The NCOM provides forecasts of the ocean state, and the Navy Coupled Ocean Data Assimilation (NCODA) uses a 3dVar algorithm to assimilate observations into the model forecast state[19].

3.1. *Numerical model and observations*

NCOM has a free-surface and is based on the primitive equations under the hydrostatic, Boussinesq, and incompressible approximations. The Mellor Yamada Level 2/2.5 turbulence models are used to parameterize vertical mixing. Most terms are treated explicitly in time, except for the propagation of surface waves and vertical diffusion, which are treated implicitly. For the present study the model was configured on two grids with homogeneous grid spacing of 3 and 10 km in the horizontal. In the vertical there were respectively 46 and 50 layers having grid steps varying between 1 m and
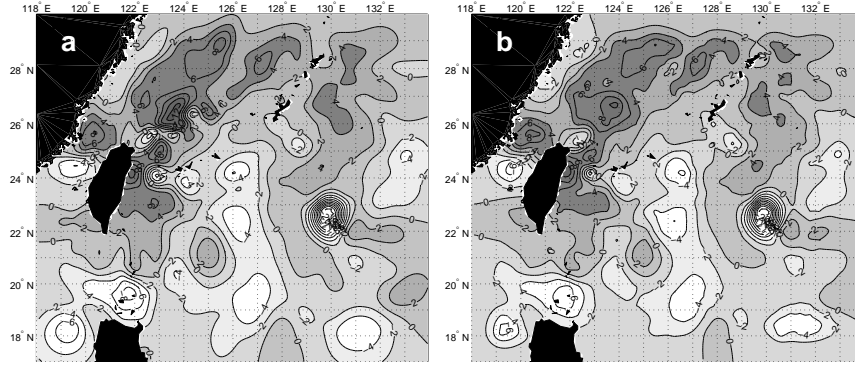
Fig. 2. The model domain and sea surface temperature increments at 10 m on Spetember 2, 2007 for the $\mathcal{C}_d$ (a) and $\mathcal{C}_2^*$ covariance models (b) (see Section 3.2). Contour interval is $0.1°$.

400 m. The number of grid points representing a 3d scalar field was $M = 10,766,576$ and $M = 862,992$ respectively. All the runs were conducted on the Dell R610 server equipped with 16 Xeon 5500 processors running at 2.8GHz.

Assimilation experiments were performed in the Okinawa Trough region (Fig. 2) in the time period from September 1 to October 31 2007. The region and time period were selected to include extensive Navy observations from an air-deployed bathythermograph survey, a shipboard hydrographic survey, and eight gliders. Observations from this Navy exercise are an addition to the standard operational data stream used by NCODA, which consists of sea surface temperature (SST) and sea surface height anomalies obtained from satellites, and temperature/salinity profiles acquired by buoys, floats, CTDs, and XBTs. The total number of observations processed during the 2-month assimilation period was 1,050,429, or approximately $\bar{N}$=17,507 points per 24-hour assimilation cycle.

3.2. Assimilation system

NCODA uses a DS 3dVar data assimilation scheme with the analysis equation (4). The vector of analysis variables **x** contains temperature, salinity, geopotential (dynamic height) and velocity fields, but in contrast to the DE approach, the BEC operator is defined by the explicit specification of its matrix elements via correlations in 3d using the correlation function shown by the dashed line in Fig. 1b. In the following, we will denote this

BEC model by $\mathcal{C}_d$, the Gaussian model and its mth-order spline approximations will be labeled by $\mathcal{C}_\infty$ and $\mathcal{C}_m$, and the asterisk will denote MS implementation (3) of the spline model ($\mathcal{C}_m^*$).

In the assimilation experiments, the $\mathcal{C}_d$ model was replaced by the tested BEC models. Several assimilation runs with $\mathcal{C}_d$ and other BEC models were also performed over the 2-month assimilation period for comparison purposes. In these runs, the horizontal decorrelation scale was set to 45 km, while vertical scale varied in z in proportion with the vertical model grid step.

Since the major goal of the present study is to compare computational efficiencies of the BEC models that are quite different, their forecast skill was monitored with respect to the operation of the NCODA system with the $\mathcal{C}_d$ BEC model whose forecast skill was used as a benchmark. This was done to ensure that the computational cost of the analysis was not reduced at the expense of reduction in assimilation quality q. The latter was estimated as the DS distance between the 24-hour model temperature/salinity forecast at observation points T_f, S_f and the observed values T_o, S_o:

$$q_T(t) = \langle (T_f - T_o)^\mathsf{T} \sigma_T^{-2} (T_f - T_o) \rangle^{1/2}, \tag{10}$$

$$q_S(t) = \langle (S_f - S_o)^\mathsf{T} \sigma_S^{-2} (S_f - S_o) \rangle^{1/2}, \tag{11}$$

where $\sigma_{T,S}$ are the observation errors and the angular brackets denote averaging over the observational locations. These DS distances were normalized to measure the forecast skill s of the tested models relative to the skill of the benchmark model $\mathcal{C}_d$.

$$s(t) = \frac{q_T(\mathcal{C}) + q_S(\mathcal{C})}{q_T(\mathcal{C}_d) + q_S(\mathcal{C}_d)} \tag{12}$$

4. Results

4.1. *Comparison of the forecast skills*

As it has been noted in Section 2, spline models are characterized by broader spectra and provide less attenuation at high spatial frequencies (Fig. 1) than the Gaussian model. This property causes a certain difference in the analyses increments (Fig. 2), which may result in substantial decrease of the overall forecast skill. The forecast skills for the 10 km and 3 km resolution configurations are shown in Figure 3. It is seen that the forecast skill of both $\mathcal{C}_\infty$ and $\mathcal{C}_2$ BEC models does not depend on the minor changes in the shape of the correlation function: The 2-month mean values shown in Fig. 3 do not differ significantly from 1. This result indicates that the analyses
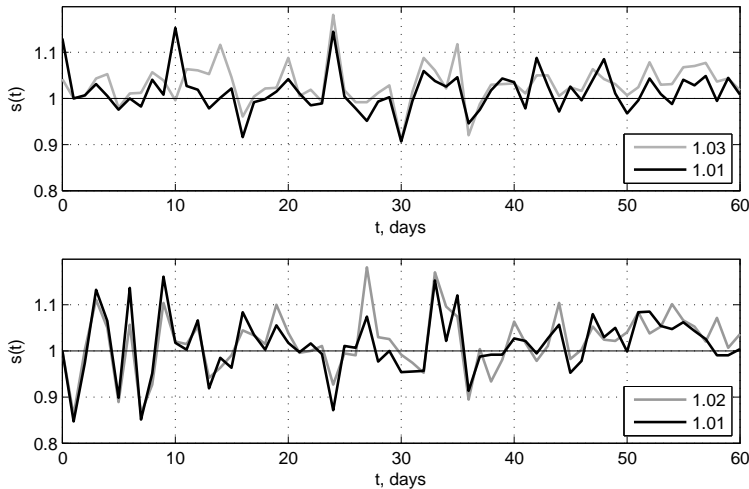
Fig. 3. Forecast skill of the $\mathcal{C}_2$ (black) and $\mathcal{C}_\infty$ (gray) BEC models implemented on coarse (10 km, above) and fine (3km, below) resolution grids. The time-averaged skills s are shown in the low right corners.

from the $\mathcal{C}_\infty$ and $\mathcal{C}_2$ models are at least not degrading the benchmark forecast generated by the operational NCODA system, while both models demonstrate similar forecast skills.

It is also remarkable that the forecast skill of the fine-resolution models appeared to be 13-15% below the skill of the respective coarse-resolution configurations. To some extent this phenomenon can be explained by the presence of small-scale motions in the 3 km configuration that are barely constrained by the available observations: On average, an observation supplies information for 610 grid points in the fine-resolution case against 110 grid points per observation for the coarse-resolution configuration.

4.2. *Comparison of the CPU times*

The dependence of CPU time was explored on both the ratio ρ of the background decorrelation scale to the grid step and on the degree of anisotropy of the correlations. A series of experiments were performed with different strengths of the anisotropy and different values of ρ for the selected date September 2, 2007 (23,970 observation points). In these experiments, the diffusion tensor was specified as follows. The background decorrelation scales ρ_i at every location were defined as a product of the local grid steps
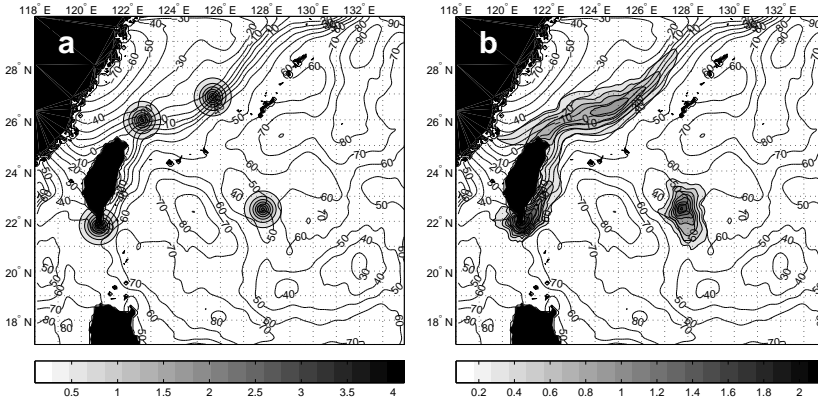
Fig. 4. Composite maps of four columns (filled contours) of the temperature correlation operator for (a) isotropic ($\lambda = 12$) and (b) anisotropic ($\lambda = 165$) cases of the $\mathcal{C}_\infty$ BEC model at 20 m. Thin contours show the SSH field. Contour interval is 10 cm.

and the universal scaling parameter ρ. The smaller principal axis in the horizontal direction (corresponding to λ_2) was set to be orthogonal to the local velocity vector $\boldsymbol{v}$. The length of the larger axis λ_1 was set to be equal to $\lambda_2 \cdot \max(1, \sqrt{|\boldsymbol{v}|/v})$, where v is a prescribed threshold value of $|\boldsymbol{v}|$. A structure like this simulates enhanced diffusive transport of model errors in the regions of strong currents on the background of isotropic error diffusion (Fig. 4). The strength of anisotropy was controlled by changing the value of v: v=10 m/s corresponds to locally isotropic diffusion (λ=12, Fig. 4a), $v = 0.2$ m/s imposed moderately anisotropic covariances ($\lambda = 50$) in regions of strong currents, and $v = 0.07$ m/s corresponds to the strongly anisotropic case ($\lambda = 165$, Fig. 4b).

In a series of experiments, NCODA observations on Spetember 2, 2007 were analyzed using the $\mathcal{C}_\infty$ and $\mathcal{C}_{1,2,3}$ BEC models in both state- and data-space formulations and the required CPU times for these analyses were compared. Results of the 10 km grid size experiments are assembled in Table 1 where larger anisotropy corresponds to the larger maximum eigenvalues λ of the diffusion operator (column 2). Respectively, the tested values of ρ correspond to the decorrelation scales of 30, 45 and 70 km.

As can be seen from Table 1, the numbers indicate improved computational efficiency of the low-order ($m < 3$) MS implementation of the spline model. For higher-order models, the MS solution appears to be less efficient due to exponential growth of the condition number of the system matrix.

Table 1. CPU times τ_∞ for the Gaussian covariance model and the relative CPU times of the mth-order spline models implemented in DS (τ_m) and in MS (τ_m^*). The accuracy of system solutions (defined as the ratio between the norms of the residual and the rhs vectors) is $\varepsilon = 10^{-6}$. The fastest cases for a given m are boldfaced.

ρ	λ	τ_∞, min	τ_m/τ_∞			τ_m^*/τ_∞		
		$\mathcal{C}_\infty$	$m{=}1$	$m{=}2$	$m{=}3$	$m{=}1$	$m{=}2$	$m{=}3$
	12	**3.47**	0.83	2.00	2.66	**0.06**	**0.31**	1.36
3.0	50	**14.9**	0.38	0.85	1.10	**0.02**	**0.21**	1.82
	165	54.0	0.16	0.32	**0.40**	**0.01**	**0.15**	1.78
	12	**8.72**	0.54	1.25	1.54	**0.04**	**0.23**	1.58
4.5	50	36.4	0.19	0.41	**0.74**	**0.01**	**0.15**	1.62
	165	156	0.09	0.21	**0.29**	**0.00**	**0.09**	1.83
	12	24.0	0.24	0.62	1.06	**0.02**	**0.16**	1.42
7.0	50	129	0.08	0.19	**0.27**	**0.00**	**0.07**	0.84
	165	418	0.04	0.11	**0.16**	**0.00**	**0.06**	6.68

Additional experiments were made on a longer time scale, with the NCODA system using the generic correlation $\mathcal{C}_d$ model as well as the tested models with 24-hour analysis cycle ($\lambda = 12, \rho = 4.5$). These experiments have shown that the $\mathcal{C}_2^*$ model is 3 times faster than $\mathcal{C}_2$ and 3.5 times faster than $\mathcal{C}_\infty$ for the 10 km configuration. Similarly, for the 3 km configuration, the $\mathcal{C}_2^*$ model was 3.3/4.2 times faster. CPU times of the $\mathcal{C}_2^*$ and $\mathcal{C}_d$ models are compared in Fig. 5. On average, the $\mathcal{C}_2^*$ model requires 30-50% more CPU time than the generic $\mathcal{C}_d$ model. However, when the number of observations exceeds $1.5\text{-}1.7 \cdot 10^4$, the $\mathcal{C}_2^*$ model appears to be more efficient. Similar computations for 3 km resolution show that this critical number of observations increases only slightly to $1.8\text{-}2 \cdot 10^4$ despite a 12-fold increase in the dimension of the model space.

5. Conclusions

The forecast skill and computational efficiency of the Gaussian and spline covariance models were examined in the framework of 3dVar assimilation of real data into an operational ocean model. It is shown that the MS formulation of the second-order spline model has similar 24-hour forecast skill and 3–5 times better computational efficiency than the DS implementation of the Gaussian and spline models. At $m < 3$, the computational efficiency of the $\mathcal{C}_m^*$ solutions is based on the low-cost computation of the action of the inverse BEC operator $\mathbf{B}^{-1} = (\mathbf{I} - \rho^2 \mathbf{D}/m)^m$ which contributes to the system matrix of the normal equation (2). On the contrary, multiplication by $\mathbf{I} - \rho^2 \mathbf{D}/m$ (or by $\mathbf{I} + \rho^2 \mathbf{D}/n$) has to be performed many times in the DS formulation to iteratively model the action of $\mathbf{B}$, which in turn is immersed
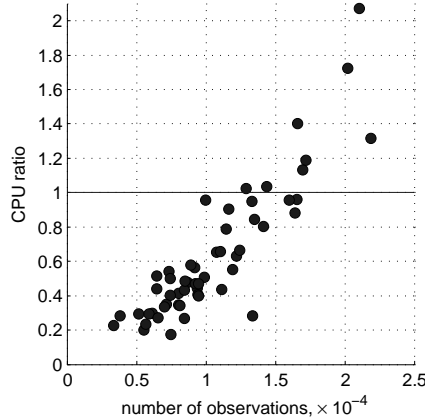
Fig. 5. CPU time ratios between the $\mathcal{C}_d$ and $\mathcal{C}_2^*$ models against the number of observations for the 10 km configuration. Points above the horizontal line correspond to the cases of the faster $\mathcal{C}_2^*$ model.

into the iterative loop required to find the solution (4) to the normal system in the DS formulation.

It is also shown, that the difference in the BEC models has a negligible impact on the forecast skill of the 3dVar assimilation system. Comparison with the benchmark NCODA 3dVar algorithm has shown that the forecast skill remains virtually the same (Fig. 3), whereas the $\mathcal{C}_2^*$ model appears to be more efficient computationally than the operational BEC model when the number of observations exceeds $15\text{-}12\cdot10^3$. Numerical experiments have also shown that spline models become especially advantageous when the background decorrelation scale is well resolved by the model grid ($\rho > 3$) and the diffusion operator is strongly anisotropic/inhomogeneous (Table 1).

The results of this work suggest that studying the applicability of the anisotropic higher-order spline BEC models to 3dVar assimilation is worth consideration for at least three reasons: 1) they are computationally efficient in processing large number of observations, 2) they are flexible enough to accommodate covariance information from the structure of the background flow, and 3) they can be easily extended to include model-generated covariances extracted from model statistics.

Acknowledgements

References

1. Gaspari, G. and S. Cohn, *Q. J. R. Met. Soc.*, **125**, 723, (1999).
2. Gaspari, G. et al, *Q. J. R. Met. Soc.*, **132**, 1815, (2006).
3. Verron, J. et al, *J. Geophys. Res.*, **104**(C3), 5441, (1999).
4. Deckmyn, A. and L. Berre, *Mon. Wea. Rev.*, **133**, 1279, (2005).
5. Pannekoucke, O., *Mon. Wea. Rev*, **137**(9), 2995, (2009).
6. Xu, Q., *Adv. Atm. Sci.*, **22**(2), 181, (2005).
7. Yaremchuk, M. and S. Smith, *Q. J. R. Met. Soc.*, **137**, in press, (2011).
8. Derber, J., and A. Rosati, *J. Phys. Oceanogr.*, **19**, 1333, (1989).
9. Purser, R.,J. et al, *Mon. Wea. Rev.*, **131**, 1536, (2003).
10. Weaver, A. and P. Courtier, *Q. J. R. Met. Soc.*, **127**, 1815, (2001).
11. Di Lorenzo, E., et al, *Ocean Modelling*, **16**, 160, (2007).
12. Pannekoucke, O. and S. Massart, *Q. J. R. Met. Soc.*, **134**, 1425, (2008).
13. Yaremchuk, M. and A. Carrier, *Mon. Wea. Rev.*, **139**, in press, (2011).
14. Ngodock, H., et al, *Mon. Wea. Rev.*, **128**, 1757, (2000).
15. Lorenc, A. C., *Q. J. R. Met. Soc.*, **112**, 1177, (1986).
16. Coutier, P., et al, *Q. J. R. Met. Soc.*, **124**, 1783, (1998).
17. Weaver, A. T., et al, *Mon. Wea. Rev.*, **131**, 1360, (2003).
18. Mirouze and Weaver, *Q. J. R. Met. Soc.*, **136**, 1421, (2010).
19. Coelho, E., et al, *J. Marine Sys.*, **78**, 5272, (2009).